Visual field representations and locations of visual areas V1/2/3 in human visual cortex

Robert F. Dougherty — Department of Psychology and Stanford Institute for Reading and Learning, Stanford University, Stanford, CA, USA

Volker M. Koch — Department of Psychology Stanford University, Stanford, CA, USA

Alyssa A. Brewer — Neuroscience Program Stanford University, Stanford, CA, USA

Bernd Fischer — Institute of Mathematics University of Lübeck, Lübeck, Germany

Jan Modersitzki — Institute of Mathematics University of Lübeck, Lübeck, Germany

Brian A. Wandell — Department of Psychology, Neuroscience Program and Stanford Institute for Reading and Learning Stanford University, Stanford, CA, USA

The position, surface area and visual field representation of human visual areas V1, V2 and V3 were measured using fMRI in 7 subjects (14 hemispheres). Cortical visual field maps of the central 12 deg were measured using rotating wedge and expanding ring stimuli. The boundaries between areas were identified using an automated procedure to fit an atlas of the expected visual field map to the data. All position and surface area measurements were made along the boundary between white matter and gray matter.

The representation of the central 2 deg of visual field in areas V1, V2, V3 and hV4 spans about 2100 mm^2 and is centered on the lateral-ventral aspect of the occipital lobes at Talairach coordinates -29, -78, -11 and 25, -80, -9. The mean area between the 2-deg and 12-deg eccentricities for the primary visual areas was: V1: 1470 mm^2; V2: 1115 mm^2; and V3: 819 mm^2. The sizes of areas V1, V2 and V3 varied by about a factor of 2.5 across individuals; the sizes of V1 and V2 are significantly correlated within individuals, but there is a very low correlation between V1 and V3.

These *in vivo* measurements of normal human retinotopic visual areas can be used as a reference for comparison to unusual cases involving developmental plasticity, recovery from injury, identifying homology with animal models, or analyzing the computational resources available within the visual pathways.

Keywords: Area V1, extrastriate cortex, cortical magnification, human

Introduction

Primary visual cortex (Brodmann's area 17; V1) can be identified using a light microscope in post-mortem material based on the heavy myelination (Stria of Gennari; Gennari, 1782). V1 has interested anatomists for more than a century, and its general position and size have been estimated many times. A surprising but consistent observation is that the surface area of V1 varies by as much as a factor of three across individuals (reviewed in Stensaas, Eddington, & Dobelle, 1974).

Andrews et al. (1997) measured the size of the lateral geniculate nucleus (LGN) and the optic tract as well as the surface area of striate cortex. They observed that the surface area correlates closely with the cross-sectional area of the optic tract as well as with the area and volume of the lateral geniculate nucleus (LGN). Given that photoreceptor density also varies by up to a factor of three across individuals (Curcio, Sloan, Packer, Hendrickson, & Kalina, 1987), it is possible that this density is a key variable that leads to the variation in size of the central representations found in the LGN and V1.

To what extent do the sizes of other visual areas follow the size of V1? This question has not been answered precisely. Amunts et al. (2000) measured the volume of Brodmann's areas 17 and 18 in ten brains

Doi:10.1167/3.10.1 Received May 30, 2003; published October 24, 2003 ISSN 1534-7362

(post-mortem). However, they did not report on a correlation between the sizes of these areas. Also, the correspondence between Brodmann's area 18 and visual area V2 is not as clear as that between striate cortex and V1.

With the ability to identify the location and size of areas V1, V2, and V3 in the living human brain, we can extend the measurements of surface area from V1 into functionally defined visual areas V2 and V3, and we can further determine how closely surface area correlates amongst these three visual areas. In this paper we describe a set of structural and functional MRI measurements of the cortical position and surface area within those portions of V1, V2, and V3 that represent the central 12 degrees of the visual field. The surface area measurements of V1 from our population agree quantitatively with several post-mortem (Amunts et al., 2000; Brodmann, 1918; Filimonoff, 1932) and lesion (Horton & Hoyt, 1991) measurements, but our measurements differ from the post-mortem measurements in Stensaas et al. (1974) and Andrews et al. (1997).

We report, for the first time, measures of the surface area of functionally defined human V2 and V3. We further report a significant correlation between the surface areas of V1 and V2 across subjects. Interestingly, the strong correlation that we measure between V1 and V2 diminishes, or perhaps is even absent, when comparing the surface area of V1 and V3. Our results, taken together with those of Andrews et al. (1997), suggest that the mature size of visual areas V1 and V2 may be traced back to the individual differences in number of ganglion cells and perhaps ultimately to individual differences in photoreceptor density. It appears that the surface area of V3, however, depends on other inputs, such as those from more central locations or from connections that pass through V2 bypassing V1 (Sincich & Horton, 2002).

We have also used functional data to measure the ratio of visual field extent represented per unit area of cortex (deg^2/mm^2). We confirm earlier measurements of the linear magnification of the central visual field in V1 (Endo et al., 1997; Engel, Glover, & Wandell, 1997; Horton & Hoyt, 1991) and we extend these measurements to two-dimensions. We further present novel measurements of the magnification in V2 and V3. In V1 and V2, the representation at 3 deg occupies roughly 16 mm^2 of cortex per square degree of visual angle; at 11 deg each square degree of angle occupies roughly 4 mm^2 of cortex. The very central fovea is difficult to estimate precisely, but is on the order of 28 mm^2 per square degree. The magnification in V3 is similar to that of V1 and V2 when the overall size difference between these areas is taken into account; similar magnification rules hold for eccentric and angular compression.

Some investigators combine responses across subjects by placing data from different brains onto a normalized brain atlas. To estimate the spatial blurring in visual cortex introduced by averaging data normalized in this way, we measured the Talairach coordinates of several functional landmarks (cortical positions defined by stimulus-driven activations). The position variability of these functional landmarks measures the spatial blurring introduced by normalization. The Talairach positions of various functional landmarks were distributed over distances exceeding one centimeter. Defining visual area positions based on a normalized atlas blurs the spatial data far beyond the instrumental resolution. For the occipital region, sulcal landmarks within an individual's brain predict the positions of functional landmarks more accurately than Talairach coordinates.

Methods

Functional magnetic resonance data were acquired on a GE 3T Signa LX scanner (GE Medical Systems, Milwaukee, WI) using a custom-built high-gain head coil. Subjects' heads were fixed throughout the measurement period by means of a bite bar or snug-fitting pads. All subjects had previous experience with functional MR scans.

Subjects viewed visual stimuli displayed on one of two systems. Most subjects viewed stimuli projected from an LCD projector onto a small rear-projection screen mounted on the head coil. This display extended 15 deg of visual angle from fixation vertically (total 30 deg), and 20 degrees (total 40 deg) horizontally.

Some of the subjects viewed stimuli displayed on an LCD display placed in a shielded box at the foot of the scanner bed and viewed through binoculars and adjustable mirrors. This display system subtended 12 degrees of visual angle from fixation vertically and 16 degrees from fixation horizontally.

Anatomical data preparation

Anatomical images were acquired on a GE 1.5T Signa LX scanner using a 3-d SPGR pulse sequence (1 echo, minimum TE, 15° flip angle, 2 excitations). Sagittal slices were acquired and the inplane voxel size was 240/256 x 240/256 mm with 1.2 mm slice thickness. The anatomical images were segmented into gray matter and white matter using custom software (Teo, Sapiro, & Wandell, 1997). To facilitate analysis and visualization of the data, the occipital lobe area of interest was computationally flattened (Wandell, Chial, & Backus, 2000).

Accurate identification of white matter is crucial for making measurements along the cortical surface. Small segmentation errors can be tolerated in fMRI studies where data are blurred and averaged across subjects. But

such segmentation errors can introduce substantial errors in the cortical surface area measurements; hence, such errors cannot be tolerated for the measurements undertaken here. Further, the occipital lobe is a particularly difficult region for automatic segmentation algorithms because it is very convoluted and has thin tendrils of white matter. For these reasons the white matter in the occipital lobe was hand-edited following the initial automatic segmentation and the data were repeatedly checked for small segmentation errors.

The following anatomical landmarks were identified by hand in the T1 anatomical images: the anterior commissure, the posterior commissure, the mid-sagittal plane, and the boundaries of cortex along each of the three axes. These points were used to transform voxel coordinates to and from Talairach coordinates (Cox, 1996; Talairach & Tournoux, 1988).

Stimuli

Visual field maps were measured using rotating wedge and expanding ring stimuli that create traveling waves of neural activity in visual cortex (DeYoe et al., 1996; Engel et al., 1997; Engel et al., 1994; Sereno et al., 1995). The specific spatial and temporal pattern of the stimulus is not important for creating retinotopic maps in early visual areas; many choices produce satisfactory maps. The wedge and ring were made of drifting, achromatic (mean luminance ~50 cd/m^2), dartboard contrast patterns (~90 % contrast) that alternately moved radially towards and away from fixation at a velocity of 1 deg per second. The wedge spanned 90 deg of angle and extended to 12 deg from fixation. The wedge completed a full rotation every 24 sec, changing positions in synchrony with the data acquisition frame rate of 3 sec (TR). The ring stimuli occupied one half of the visual field (50% duty cycle), completed a full expansion every 24 sec, and changed eccentricity position in synchrony with the 3 sec TR. Figure 1 illustrates this retinotopy paradigm.

Functional MR

Functional MR data were acquired with a spiral pulse sequence (Glover, 1999; Glover & Lai, 1998) with 21-30 obliquely oriented slices acquired every 3 seconds (TE: 30 ms, TR: 1.5 s, 2 interleaves, 70 deg flip angle, effective voxel size: 2x2x3 mm). Each individual functional scan lasted about 4 minutes and subjects were given a brief break between scans. A set of 2D fast SPGR anatomy images was acquired before the series of functional scans. These T1-weighted slices were physically in register with the functional slices and were used to align the functional data with the high-resolution

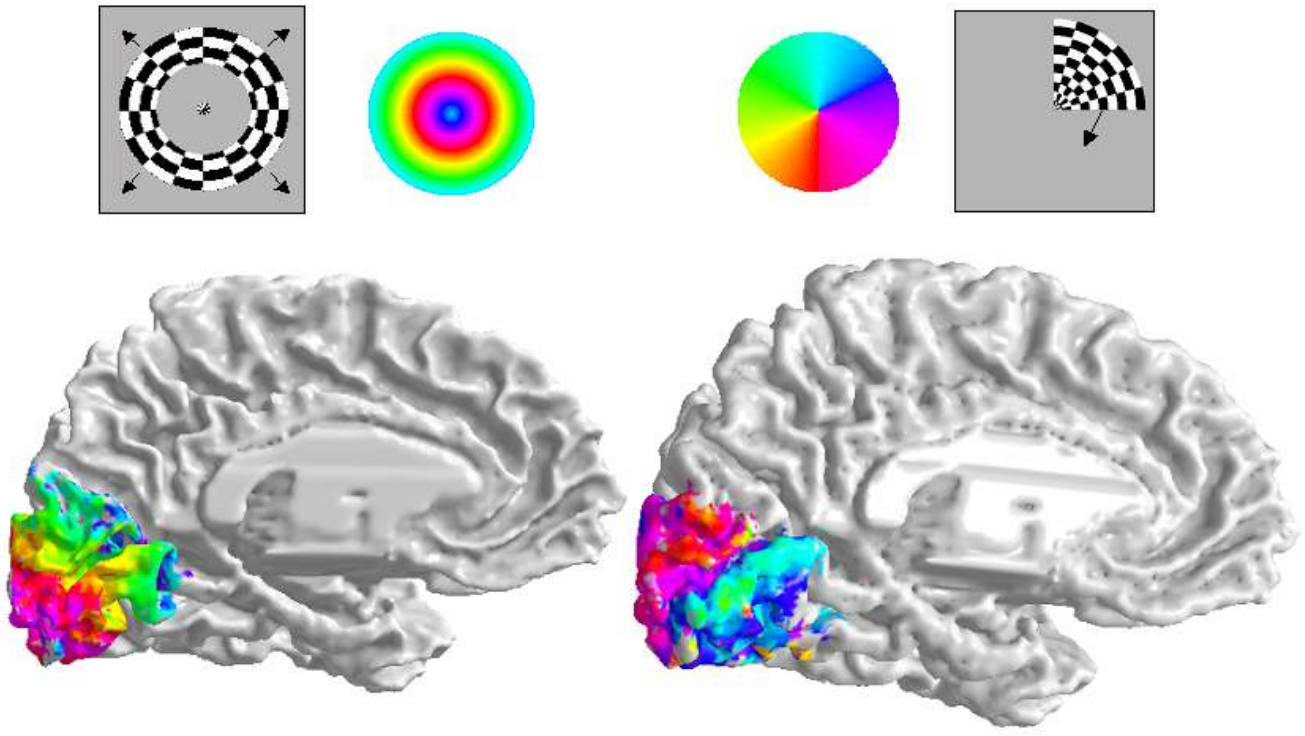

Figure 1. The Retinotopy paradigm. Two stimuli are used to measure the retinotopic maps in cortex. Expanding ring stimuli map eccentricity and rotating wedge stimuli map polar angle. The phase of the best-fitting sinusoid for each voxel indicates the position in the visual field that produces the maximal activation for that voxel. Thus, these pseudo-color phase maps are used to visualize the retinotopic maps. Data are shown for the left hemisphere of one subject.

anatomy data via a semi-automated 3D coregistration algorithm (Nestares & Heeger, 2000).

The functional data were inspected for unwanted head movements. Small movements were corrected via standard motion correction algorithms (Nestares & Heeger, 2000). In the very few cases of a large motion artefact, the data were discarded. The time series from multiple measurements of the same stimulus were averaged.

Visualization and preparation of the measurements can be simplified by working on 2-dimensional 'flattened' representations of the cortical manifold. These flat maps allow for easy specification of regions of interest and simplify the process for finding visual areas (described below). Because the flattening process inevitably distorts distance and area measurements, all surface area and distance measurements were made in the 3-d cortical manifold by mapping the 2-d coordinates back to the 3-d manifold.

We used a custom automated algorithm to find the boundaries of visual areas. This algorithm includes a model of the expected pattern of activity in the retinotopic cortex (the 'atlas'). This atlas was transformed to fit the data using a technique that simulates rubber-sheet deformation. With this technique, we obtain an objective map of each individual's early retinotopic visual areas. Details of this algorithm are described in the Appendix.

Surface area measurements

All surface area measurements were made on the 3-d cortical manifold. To measure surface area, a functionally defined region of interest (ROI) was identified on a 2-d flat map. For all measurements except the foveal confluence, the ROIs were created automatically using the atlas software described in the Appendix. The foveal confluence was identified by hand as the atlas does not attempt to model this functional landmark. After identification on the flat map, the ROI consists of a set of 2-d coordinates on a rectilinear grid. For each of these flat map coordinates, we find the nearest node on the mesh that describes the boundary of the white-gray matter interface. The set of mesh nodes in the ROI are the vertices of the set of triangles that form the patch on the 3-d cortical manifold that corresponds to the ROI. The surface area of the ROI is simply the sum of the area of each of the n triangles. This area can be measured using Heron's formula:

$$Area = \sum_{i=1,n} \sqrt{s_i(s_i - a_i)(s_i - b_i)(s_i - c_i)} \quad (1)$$

where a, b and c are the lengths of the three edges of each of the *n* triangles and

$$s_i = \frac{(a_i + b_i + c_i)}{2}. \quad (2)$$

We measured surface area along the boundary between gray and white matter; using our methods this boundary is identified more reliably than the outer surface of the gray matter or any particular cortical layer (Teo et al., 1997).

Results

V1/2/3 sizes and correlations

Table 1 contains measurements of the surface area of the visual field representations from 2-12 deg. Right and left hemispheres, (left and right visual field) as well as dorsal and ventral aspects (lower and upper visual field) are listed separately for each subject.

Table 1 also contains surface area measurements of the large central representation (0-2 deg). This cortical region falls at the confluence of areas V1, V2, V3 and hV4. The surface area of the central representation is shown as a single measurement because we did not separate the visual areas within this region.

Left hemisphere V1 surface area (mean = 1578 mm^2) tended to be larger than right hemisphere V1 area (mean 1362 mm^2). This difference was significant (pairwise $t = 2.39$, $p = 0.033$, $df = 13$). There were no significant differences between left and right V2 (means 1187 mm^2 and 1044 mm^2, respectively) or between left and right V3 (means 831 mm^2 and 808 mm^2, respectively).

The surface areas of corresponding visual areas in the two hemispheres of the same subject are correlated. This correlation was quite strong for V1 ($r = 0.744$, $p = 0.001$, $df = 11$) and the foveal confluence ($r = 0.863$, $p = 0.009$, $df = 4$). However, it was weaker for V2 ($r = 0.455$, $p = 0.104$, $df = 11$) and V3 ($r = 0.349$, $p = 0.227$, $df = 11$). The strong correlation between the two hemispheres for V1 agrees with the post-mortem data of Andrews et al. (1997).

Across all the visual areas, dorsal regions (799 mm^2, 597 mm^2, 435 mm^2 for V1, V2 and V3) tended to be larger than ventral regions (671 mm^2, 518 mm^2, 384 mm^2 for V1, V2 and V3). This difference was significant in V1 (pairwise $t = 3.24$, $p < 0.01$, $df=13$), but not in V2 or V3.

A scatter plot comparing the surface areas of V1 and V2 (Figure 2) shows a relatively high correlation ($r = 0.621$, $p < 0.001$, $df = 25$). The V2 surface area in the 2-12 deg representation is roughly 75% that of V1, and this size difference is statistically significant (pairwise $t = 3.74$, $p < 0.001$, $df = 27$). As reviewed by Sincich and Horton (2002), V2 receives significant input from both V1 and the pulvinar. Hence, the reduced size of V2 suggests that it may only receive a portion of the V1 output or that it has a more efficient representation of this output.

No significant correlation was found between the surface area of V1 and V3 ($r = 0.03$, $p = 0.879$, $df = 25$). However, V3 was on average 56% the size of V1, and this difference was significant (pairwise $t = 6.76$ ($p<0.001$, $df=27$).

Despite the lack of a correlation between V1 and V3, the surface area of V2 was correlated with the area of V3 ($r = 0.513$, $p = 0.006$, $df = 25$).

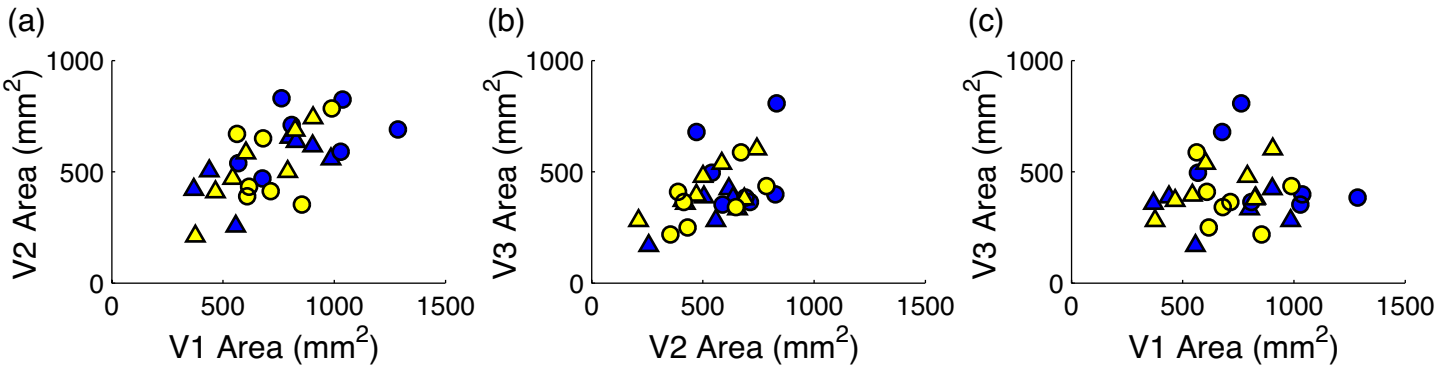

Figure 2. V1 surface area correlates with V2 surface area (a), but V3 surface area is only weakly correlated with V2 surface area (b) and there is no significant correlation with V1 surface area (c). Note that these are measurements of quarter-field cortical representations. Triangles are ventral regions and circles are dorsal regions; yellow symbols are right hemisphere data and blue symbols are left hemisphere data.

Table 1. Surface Area Measurements.

			Ventral			Dorsal			Total		
Subject	**Hemi.**	**Fovea**	**V1**	**V2**	**V3**	**V1**	**V2**	**V3**	**V1**	**V2**	**V3**
RFD	left	1165	369	421	359	567	540	495	936	962	854
RFD	right	1362	466	411	371	608	389	409	1074	800	780
BAW	left	2878	903	617	424	1038	825	401	1941	1442	824
BAW	right	2940	825	687	378	988	786	435	1813	1473	813
ARW	left	1989	985	558	281	1286	692	383	2271	1250	664
ARW	right	2084	905	743	603	853	355	219	1758	1098	822
PN	left	1728	439	505	387	809	710	364	1248	1215	751
PN	right	2445	603	585	538	617	432	251	1220	1018	789
JR	left	982	557	257	169	679	470	680	1236	726	849
JR	right	1849	376	211	281	713	414	365	1089	625	646
SHL	left	1993	800	656	334	763	830	807	1563	1486	1141
SHL	right	2562	544	471	395	563	672	587	1106	1142	982
AAB	left	2475	829	636	382	1028	589	353	1857	1226	735
AAB	right	2884	791	501	480	680	649	341	1470	1150	821
	mean:	**2095**	**671**	**518**	**384**	**799**	**597**	**435**	**1470**	**1115**	**819**
	median:	**2039**	**697**	**531**	**380**	**738**	**619**	**392**	**1359**	**1146**	**817**
	stdev:	**638**	**214**	**155**	**109**	**215**	**165**	**161**	**403**	**269**	**124**
	sem:	**177**	**59**	**43**	**30**	**60**	**46**	**45**	**112**	**75**	**34**
	min:	**982**	**369**	**211**	**169**	**563**	**355**	**219**	**936**	**625**	**646**
	max:	**2940**	**985**	**743**	**603**	**1286**	**830**	**807**	**2271**	**1486**	**1141**

Surface area measurements for the 2-12 deg visual field representation of V1, V2 and V3 as well as the central representation (0-2 deg) at the confluence of V1, V2, V3 and hV4 ("Fovea"). The measurements are shown for right and left hemispheres, dorsal and ventral aspects of V1/2/3, and seven different subjects (14 hemispheres). Various summary statistics are listed at the bottom of the table.

Cortical magnification

The cortical surface area (mm^2) per degree of visual field (deg^2) decreases systematically with eccentricity (Figure 4). This is also illustrated in Figure 3. As illustrated in Figure 5, these functional MRI estimates of cortical magnification are in good agreement with the estimates based on human lesion and corresponding visual field defect measurements from Horton and Hoyt (1991). Note that this excellent quantitative agreement involves a comparison between two very different kinds of measurements.

The cortical magnification functions did not differ significantly between left and right hemispheres or between ventral and dorsal cortex after normalizing for total surface area. Thus, the unnormalized data shown in Figure 4 were normalized and combined across left/right and ventral/dorsal measurements. The resulting magnification curves for V1, V2 and V3 are shown in Figure 5. The curves for all three areas are similar in shape, with the downward offsets for V2 and V3 reflecting their smaller total surface area relative to V1.

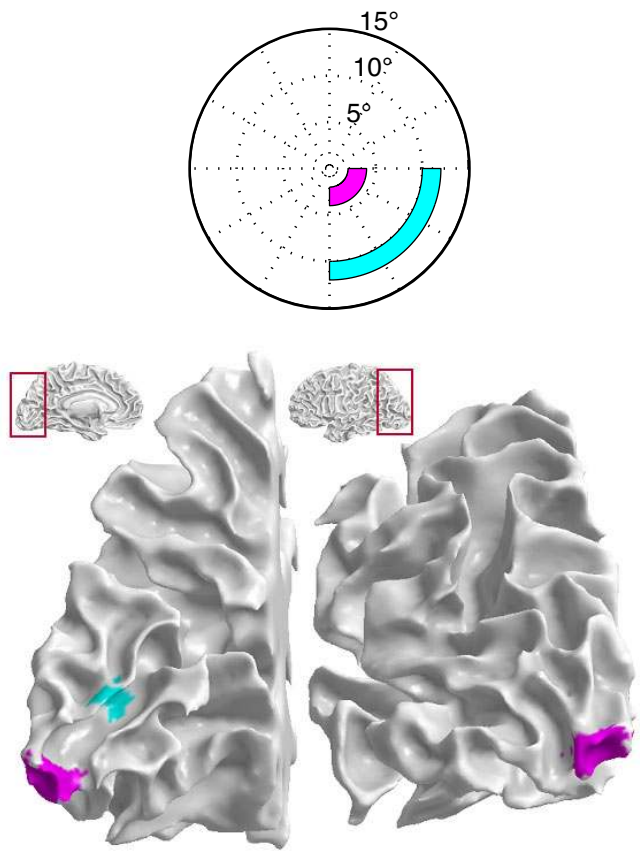

Figure 3. Graphical representation of cortical magnification. The top panel shows the visual field area covered by two arcs in the lower right visual field, one spanning 2-4 degrees eccentricity and another spanning 10-12 degrees. The bottom panel includes two views of the same brain, showing the representation of these areas on the cortical surface in V1.

The cortical magnification functions for individual hemispheres shown in Figure 5 have been normalized by mean surface area to remove the considerable inter-individual variance in total surface area (see Table 1). This normalization does not affect the shapes of the functions, but it scales each curve vertically to match the group mean surface area for that visual area.

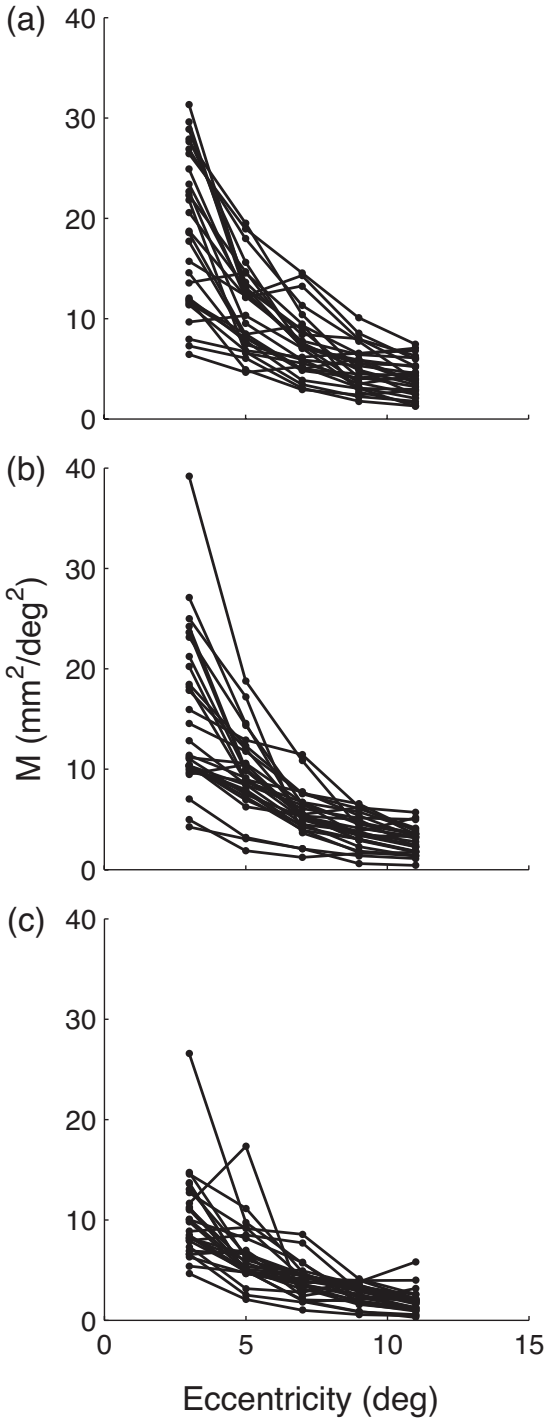

Figure 4. Surface area cortical magnification functions for all hemispheres. (a) V1, (b) V2 and (c) V3.

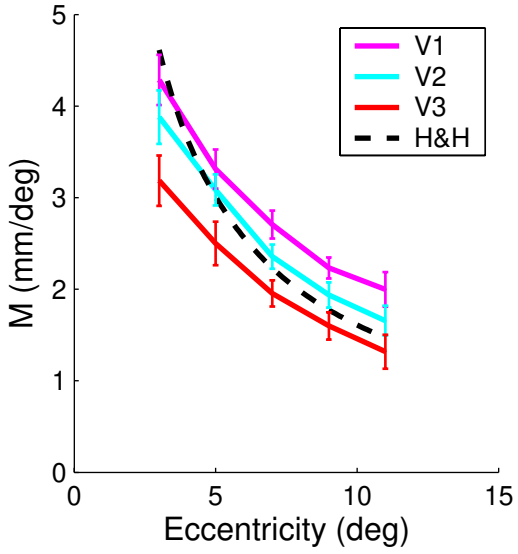

Figure 5. Conventional (linear) cortical magnification functions from the current data, collapsed across all hemispheres, compared with data from Horton and Hoyt.

Visualization of V1, V2 and V3

Figure 6 shows the size and position of that portion of V1 that represents the visual field from two to twelve degrees of eccentricity. The data are shown from three subjects that illustrate the range of locations and sizes. While this region of V1 always falls near calcarine cortex, the location and shape of calcarine varies considerably across subjects. For example, the V1 representation extends significantly onto the ventral and lateral surface in subject ARW but much less so in the other two subjects. The total surface area for ARW is roughly 1.2 times the surface area for subject AAB and 2.4 times that of subject RFD.

The upper and lower vertical meridian representations fall within about 1 cm of the lower and upper banks of the calcarine sulcus, but the registration with these anatomical landmarks is not precise in all hemispheres.

Figure 6 also shows the size and positions of areas V2 and V3. Figure 6 is accompanied by a QuickTime VR animation of one set of data.

Visualization of the foveal confluence

We did not attempt to distinguish between V1, V2 and V3 in the central 2 degrees of the retinotopic map. We refer to this part of the map as the 'foveal confluence'. Surface area measurements of this region are presented in Table 1. Interestingly, the right foveal confluence (mean = 2323 mm^2) tended to be larger than the left (mean = 1887 mm^2). This difference was significant (pairwise t = -3.39, p=0.015, df=6) and is opposite of the left hemisphere bias that we observed in V1.

Figure 7 shows the size and position of the foveal confluence in several representative subjects. As expected, the foveal confluence lies on or near the occipital pole. In some subjects, however, it extends quite far on the lateral-ventral surface.

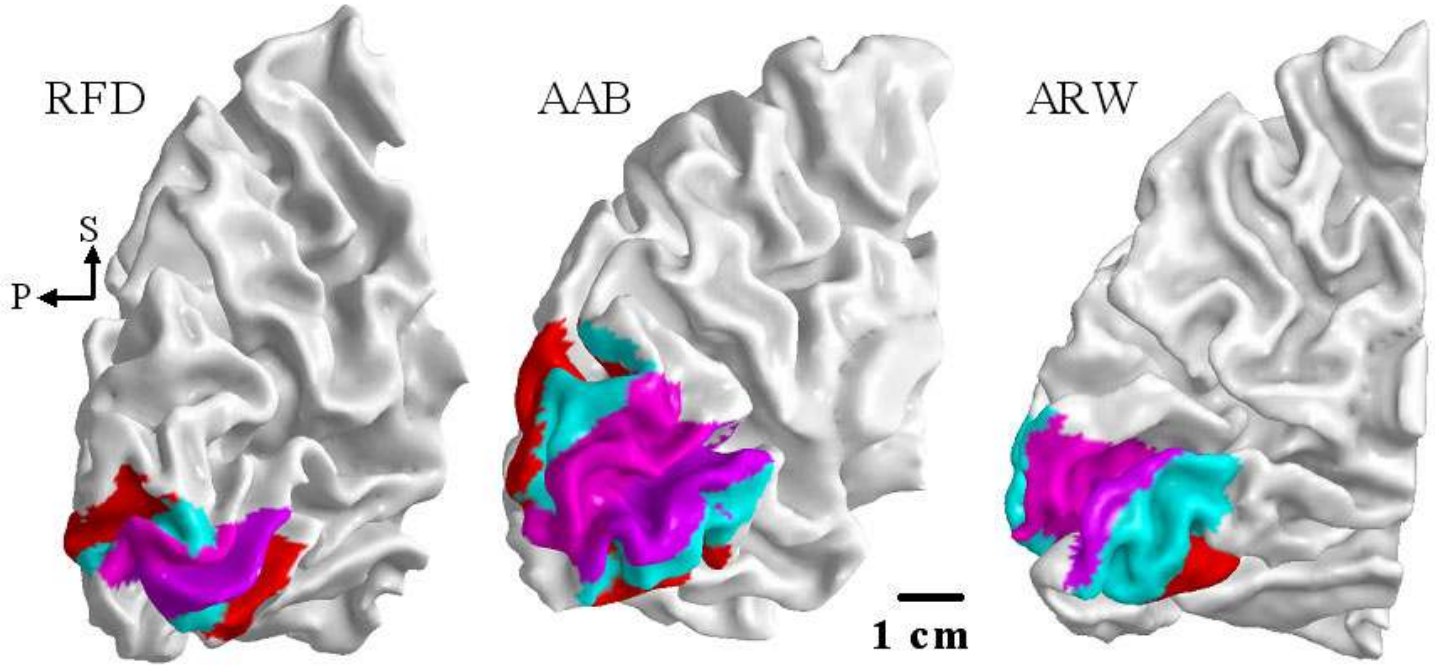

Figure 6. Position and size of the 2-12 degree region of V1, V2 and V3 in three hemispheres. The color convention is the same as in Figure 5: V1 is indicated by magenta, V2 by cyan and V3 by red. Click on the image to see a QuickTime VR animation.

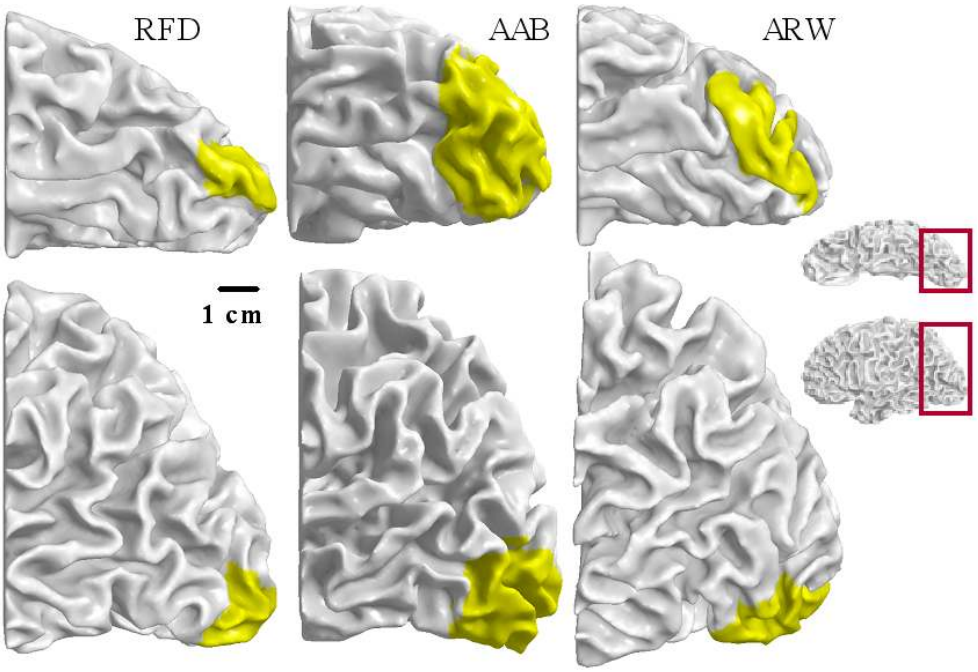

Figure 7. Position and size of the foveal confluence in three hemispheres. The ventral surface is shown in the upper row and the lateral surface is shown in the lower row.

Stereotaxic coordinates

The variability of visual area positions with respect to stereotaxic atlas coordinates has been documented in several recent studies (Amunts et al., 2000). Table 2 shows the variance of several functional landmarks in areas V1, V2 and V3 with respect to Talairach coordinates. These landmarks include the center of mass of the foveal confluence and the 12-degree eccentricity representations on the horizontal meridia within V1 as well as the ventral and dorsal V2/V3 borders. These coordinates are shown graphically on the canonical single-subject T1 brain from SPM99 (Figure 8).

The variance of these stereotaxic coordinates along any single axis exceeds a centimeter and the range exceeds two centimeters. The mean Euclidean distance between the confluence landmark positions for each pair of subjects is 14mm. For the 12-degree horizontal meridia the mean separations were 15mm (V1) 12mm (ventral V2/3), and 18mm (dorsal V2/3). The maximum separations between subjects for these landmarks were 28mm, 32mm, 27mm and 40mm. This analysis confirms the reported variability (Amunts et al., 2000; Dumoulin, Baker, & Hess, 2001) and adds specificity by measuring the specific visual field representations rather than a central measure of an entire visual area. Positional variability may be reduced by alternative nonlinear spatial normalization procedures (see e.g., Crivello et al., 2002), but even an optimistic assessment suggests that such co-registration is inappropriate for studies in which spatial resolution should be precise to within a few millimeters.

Discussion

Related literature

In human, as in macaque, the surface area of V2 is about 70-80% that of V1 (Brewer, Press, Logothetis, & Wandell, 2002). Area V3 is relatively large in human compared to macaque, spanning roughly 60% the surface area of V1. Recent fMRI estimates of the macaque visual areas suggest that V3d+V3v is roughly 40% the size of V1 (Brewer et al., 2002) although anatomical measurements suggest that the ratio is as low as 13% (Van Essen, personal communication, 2003; Van Essen et al., 2001; Van Essen, Newsome, Maunsell, & Bixby, 1986).

A potential source of bias in our estimates of the surface area is the initialization of the atlas. The atlas was initialized to approximate the data (measured by eye), and this was close to a V3 /V1 surface area of 40-60%. This initialization does not constrain the result because the fitting algorithm iterates roughly 20-80 steps and there is no memory of the error between iterations. Thus, the relative sizes of the regions in the final atlas fits can deviate quite significantly from the initial atlas estimates (see Appendix for atlas fitting details). Therefore, we believe that the difference in the ratio of V3/V1 surface area between humans and macaque is real. The size difference may reflect a functional divergence between these two species (Tootell et al., 1997).

Visual areas V1, V2 and V3 are difficult to distinguish using fMRI in a region that represents the central visual field (1-2 deg). The cortical surface area of this foveal confluence spans approximately 2100 mm^2 of cortical surface area in each hemisphere. The surface area of this central representation alone exceeds that of the cortical region representing the entire central 11 deg in macaque (Brewer et al., 2002).

Several groups have measured the volume or surface area of human area 17. Most recently, Amunts et al. (2000) measured cytoarchitectonic maps of areas 17 and 18 in human cortex from serial histological sections; they then transferred these maps into a stereotaxic coordinate system on a reference brain (Roland & Zilles, 1994, 1996, 1998).

Amunts et al. estimated the combined volume of Area 17 (left and right) to be 23.3 cm^3. Assuming an average cortical thickness of 2.5 mm (Fischl & Dale, 2000), the area 17 surface area in each hemisphere is 4660 mm^2. This value is roughly double the average V1 surface area estimated by Stensaas et al. (1974) (2,134 mm^2) and Andrews et al. (Andrews et al., 1997); indeed, this estimate is higher than the largest V1 in the Stensaas et al. sample (3,702 mm^2). The value is only slightly higher than the estimates from Brodmann (1918) and Filimonoff (1932).

The average surface area of the present functional measurements is 1470 mm^2, and this represents only that portion of V1 representing 2-12 deg. The average surface area of the foveal confluence of V1, V2, V3, hV4 is 2100 mm^2, and we estimate that 33% of the foveal confluence is within V1. Hence, we estimate the surface area of V1 representing the central twelve degrees to be 0.33(2100 mm^2) + 1470 mm^2 = 2163 mm^2. These estimates are inconsistent with Stensaas et al. and Andrews et al. who describe the entire surface area of V1 to be approximately this size. If the central 12 deg represents roughly 50-60% of the entire surface area of V1 (Horton & Hoyt, 1991), then the present estimates are consistent with those of Amunts et al., Brodmann and Filimonoff (Amunts et al., 2000; Brodmann, 1918; Filimonoff, 1932).

We note that all of the studies agree that there is substantial variance in surface area between subjects. The main difference between studies is the estimated absolute surface area; this quantity is very difficult to measure precisely in anatomical preparations.

Several groups have estimated the cortical magnification function using fMRI, visual evoked potentials and psychophysics (see (Slotnick, Klein,

Table 2. Talairach Coordinates.

		Confluence			V1 12deg HM			Ventral V2/3 12deg HM			Dorsal V2/3 12deg HM		
Subject	**Hemi.**	**X**	**Y**	**Z**	**X**	**Y**	**Z**	**X**	**Y**	**Z**	**X**	**Y**	**Z**
RFD	left	-22	-93	-25	-6	-79	-12	-12	-73	-13	-2	-91	-8
RFD	right	20	-96	-18	11	-82	-3	10	-76	-16	13	-94	7
BAW	left	-22	-86	-4	-9	-68	9	-14	-65	-4	-7	-82	29
BAW	right	18	-90	-20	12	-83	7	13	-66	-12	8	-88	27
ARW	left	-36	-86	-17	-20	-76	7	-12	-70	-7	-27	-92	15
ARW	right	27	-88	-4	3	-85	5	5	-72	-3	9	-85	17
PN	left	-34	-92	-11	-15	-80	0	-24	-70	-3	-14	-96	11
PN	right	32	-89	-8	8	-70	5	16	-66	-5	14	-86	11
JR	left	-41	-86	-6	-20	-59	8	-21	-58	2	-10	-74	20
JR	right	31	-89	-3	16	-66	13	14	-55	0	1	-76	21
SHL	left	-22	-86	-13	-14	-68	13	-17	-62	-1	-14	-72	25
SHL	right	20	-93	-12	9	-75	7	14	-63	-5	1	-80	20
AAB	left	-26	-97	-12	-17	-75	2	-11	-71	-7	-18	-89	13
AAB	right	26	-95	-5	16	-76	2	8	-70	-6	9	-83	17
left mean:		**-29**	**-78**	**-11**	**-13**	**-63**	**3**	**-14**	**-59**	**-4**	**-12**	**-75**	**13**
right mean:		**25**	**-80**	**-9**	**9**	**-67**	**5**	**10**	**-59**	**-6**	**7**	**-74**	**15**
left stdev:		**8**	**5**	**7**	**5**	**8**	**8**	**5**	**5**	**5**	**8**	**9**	**12**
right stdev:		**6**	**3**	**7**	**5**	**7**	**5**	**4**	**7**	**5**	**5**	**6**	**7**

Talairach coordinates specifying the center of mass of the foveal confluence for each hemisphere are listed, as well as the coordinates for the 12 degree eccentricity point along three horizontal meridia (HM)- the HM of V1, the HM of the dorsal V2/V3 border, and the HM of the ventral V2/V3 border. Following the Talairach convention, X is left/right, Y is anterior/posterior, and Z is inferior/superior. All values specify distances from the anterior commissure in mm.

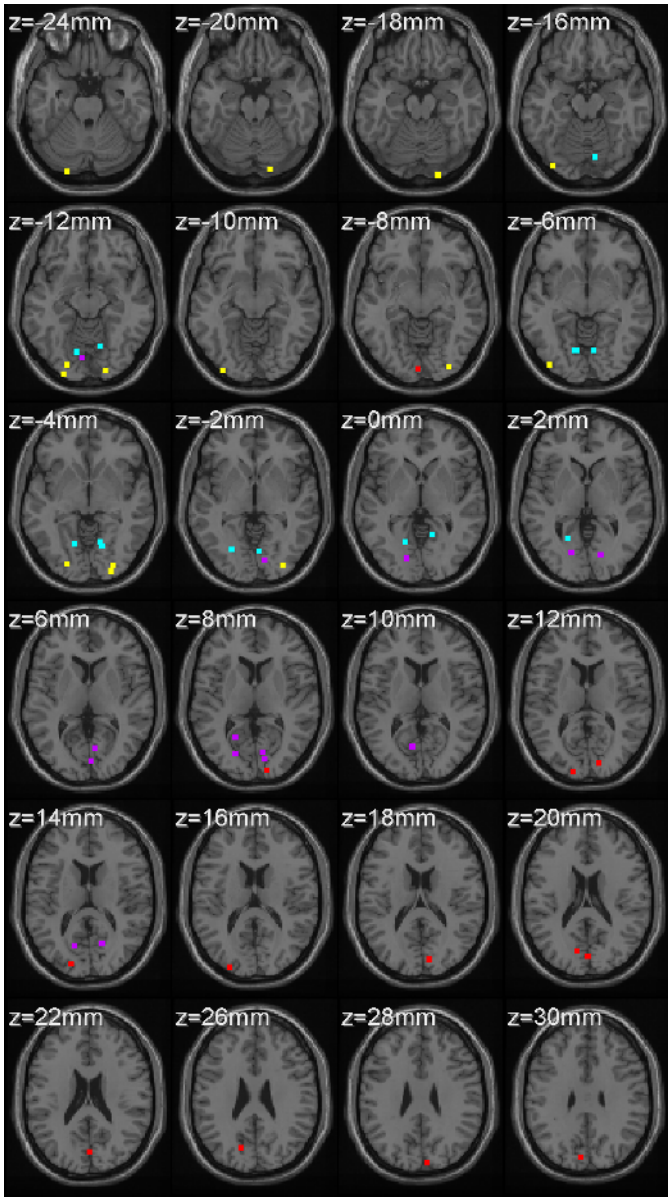

Figure 8. Talairach coordinates of four landmarks rendered on the SPM99 single-subject brain. The foveal confluence is yellow, the 12-degree eccentricity points along the horizontal meridia are: cyan (V1), magenta (ventral V2/3) and red (dorsal V2/3).

Carney, & Sutter, 2001) for a review). To fit their lesion measurements, Horton and Hoyt (1991) adapted a function used to describe cortical magnification estimates in monkey cortex:

$$M_{linear} = \frac{A}{E + e2} \quad (3)$$

where E is the eccentricity in degrees, A is the cortical scaling factor (in mm) and e2 represents the eccentricity (in degrees) at which a stimulus subtends half the cortical distance that it subtends at the fovea. Horton and Hoyt proposed that human e2 should be set to 0.75, identical to the value used to fit monkey data. They also proposed that A is 17.3 - also adapted from monkey data but adjusted to reflect the size differences between monkey and human V1.

This functional form fits the present data well. However, the parameters fit to the group data differed: the best fits are A=29.2mm, e2=3.67° for V1, A=22.8mm, e2=2.54° for V2, and A=19.4mm, e2=2.69° for V3. Because we did not measure eccentricities closer than 2°, the e2 estimates are not robust. Also, the variance across individuals is large, especially at very central locations (see Figure 4).

Volume estimation from surface area

Were the cortical surface a plane, one could calculate the gray matter volume from the surface area and knowledge of the mean cortical thickness. The cortical surface is not flat, and in regions of high curvature the local volume can differ measurably from the estimate based on planarity. Specifically, volume is underestimated on the crowns of gyri and overestimated in the fundi of sulci.

For large regions that include sulci and gyri, these two errors tend to cancel one another. For smaller regions these two types of errors may not cancel well. In a subset of the regions reported in this paper, we calculated the difference between estimates of gray matter volume assuming planarity and estimates that account for local curvature. The difference between the two estimates never exceeded 5 percent, even in small regions such as V3 or the sub-regions used to estimate cortical magnification. Hence, for the regions we report here, it is reasonable to estimate the gray matter tissue volume as surface area multiplied by cortical thickness.

Relationship between V1, V2 and V3

There is consensus that large variations in the size of primary visual cortex exist. Further, Andrews et al. (Andrews et al., 1997) found a correlation between the surface area of V1 and the size of the retinal and geniculate input streams. Hence, the variation of the V1 surface area might be due to the variation of the density of the photoreceptor sampling mosaic (Curcio et al., 1987; Curcio, Sloan, Kalina, & Hendrickson, 1990).

The variation in visual area size extends to V2 and V3, but is reduced. While the correlation in size between V1 and V2 is significant, the covariation between V1 and V3 is not. The correlation between V1 and V3 may be lost because of the influence of additional factors, such as the insertion of a significant pulvinar input at the level of V2 (Sincich & Horton, 2002) and increasing significance of feedback and other projections.

Size and performance

Does surface area correlate with performance? Duncan and Boynton (2002) have reported a correlation

between cortical magnification estimates (based on surface area) and a visual acuity task. If such a correlation is observed in several contexts, then a theory relating the size of the neuronal substrate, say based on signal-to-noise ratio, may become accepted. Should this connection become secure, then the analysis of correlation between surface area and performance may provide a means for uncovering the functional role of visual areas.

Appendix: Atlas fitting algorithm

Visual area locations were identified by fitting a quantitative model of the expected pattern of activation (the atlas) to the measured data. This atlas consists of two images that represent the expected pattern produced by (a) the rotating wedge stimulus and (b) the expanding ring stimulus (see Figure 1). Fitting a model of the full template has several advantages over defining only the boundaries of the visual area, which is often done by hand from the raw data or using the visual field sign map (Sereno, McDonald, & Allman, 1994). The advantages of the automating the full template fit include:

- The atlas fits both the wedge and ring data simultaneously, something that is very difficult for a human expert to do.
- The atlas allows us to define specific points within the retinotopic map, such as “the 12 degree eccentricity point along the horizontal meridian in V1”. Such local regions are not estimated by boundary definitions, and they are difficult to define on the noisy raw data. The atlas fit provides an accurate estimate of such local regions because it relies on a globally optimized fit.
- The atlas fit facilitates measurements of visual field map properties, such as surface area and cortical magnification.

The atlas-fitting algorithm has its limits and a human expert must monitor the process to ensure accurate results. The initial atlas is essentially a periodic image; the fitting algorithm can yield incorrect 'local' solutions and is sensitive to the initial position of the atlas. Thus, our procedure involves a human expert initializing the atlas position and size. The automated elastic deformation refines the fit to minimize the error between the atlas and the data. The human expert monitors this process and adjusts the atlas and/or the deformation algorithm parameters (if necessary) to ensure that the data are not over-fit and that the fit does not find incorrect local solutions.

Representative atlas fits are shown in Figure 9 (fits for all subjects are available in the auxiliary file rawDataImages.pdf). Note that most of the regions of high error within our 2-12 degree sub-region reflect discontinuities in the retinotopic map. If we assume that the true retinotopic map is smooth and continuous, then these regions most likely reflect noise in the data and the fitted atlas is a better indicator of the true retinotopic map than the raw data.

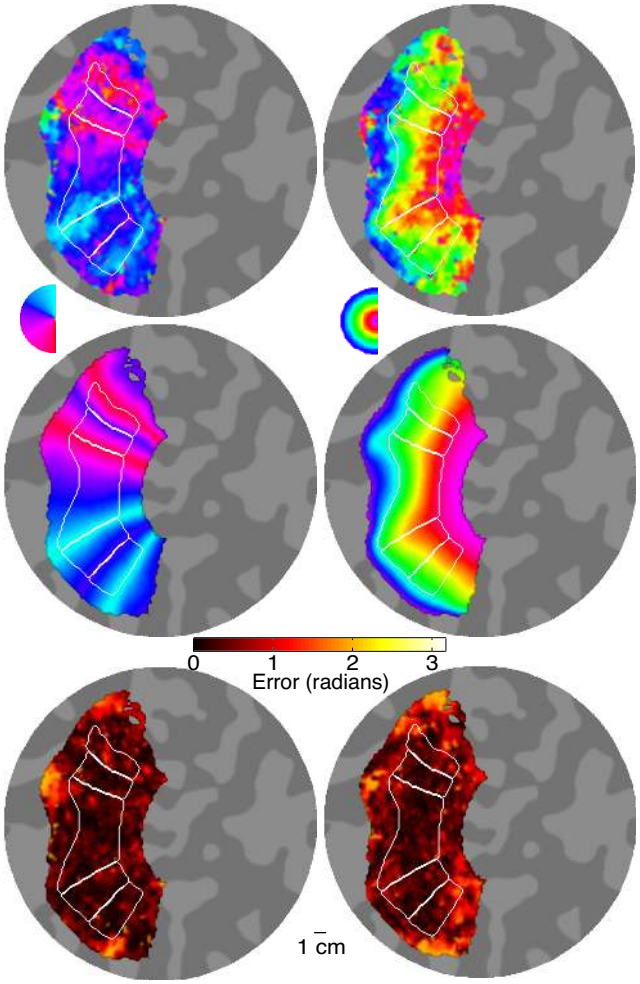

Figure 9. Atlas fit for a representative dataset. The top row shows the original data for both the rotating wedge (left) and expanding ring (right) stimuli. The middle row shows the final atlas fit to these data. Error maps for the atlas fit are computed as the absolute value of the difference between the original data and the atlas fit at each pixel. These are shown in the bottom row. The visual area boundaries computed from the atlas are show in white on all images.

The elastic deformation is based on a fast non-linear coregistration technique (Fischer & Modersitzki, 1999). The two atlases are jointly deformed to fit the data. In a pre-registration phase, an optimal affine linear deformation is computed. The second phase is based on elastic theory. Here, a non-linear deformation is computed, which on one hand mimics an elastic material

and on the other hand minimizes the differences between the templates and the data. The optimal deformation (u,v) minimizes the weighted sum of the error (*error*, external forces) and the elastic potential (P, internal forces) of the deformation:

$$error(u,v) = \int (T(x-u(x,y),y-v(x,y)) - R(x,y))^2 d(x,y), \quad (4)$$

$$P(u,v) = \int \frac{\lambda}{2}\left(u_x + v_y\right)^2 + \mu\left[u_x^2 + v_y^2 + \frac{1}{2}\left(u_y + v_x\right)\right] d(x,y). \quad (5)$$

Successive deformations are computed and applied to the templates. These deformed templates become the templates for the next iteration. Thus, the algorithm has no memory. For this reason, the final fitted template can deviate markedly from the initial template without significant penalty.

Software for creating the atlas and performing the elastic deformation to fit the data can be found in the auxiliary files. The Matlab function makeRetinotopyAtlases.m was used to build the initial atlases given a set of four user-defined landmark points. The Matlab function eMatching2.m was used to elastically deform the atlases to more closely match the data (jmfft.m and updateTinC.c are utility functions needed to run eMatching2.m).

Acknowledgments

Supported by National Institutes of Health Grants EY-03164 (BAW) and RR 09784. We thank Holly Bridge, D.C. Van Essen, and W. T. Newsome for their comments.

Commercial relationships: None.

References

Amunts, K., Malikovic, A., *Mohlberg*, H., Schormann, T., & Zilles, K. (2000). Brodmann's areas 17 and 18 brought into stereotaxic space-where and how variable? *Neuroimage, 11*(1), 66-84. [PubMed]

Andrews, T. J., Halpern, S. D., & Purves, D. (1997). Correlated size variations in human visual cortex, lateral geniculate nucleus, and optic tract. *Journal of Neuroscience, 17*(8), 2859-2868. [PubMed] [Article]

Brewer, A. A., Press, W. A., Logothetis, N. K., & Wandell, B. A. (2002). Visual areas in macaque cortex measured using functional magnetic resonance imaging. *Journal of Neuroscience, 22*(23), 10416-10426. [PubMed]

Brodmann, K. (1918). Individuelle Variationen der Sehsphäre und ihre Bedeutung für die klink der Hinterphauptschüsse. *Allgz Psychiat (Berline), 74*, 564-568.

Cox, R. W. (1996). AFNI: software for analysis and visualization of functional magnetic resonance neuroimages. *Computers and Biomedical Research, 29*(3), 162-173. [PubMed]

Crivello, F., Schormann, T., Tzourio-Mazoyer, N., Roland, P. E., Zilles, K., & Mazoyer, B. M. (2002). Comparison of spatial normalization procedures and their impact on functional maps. *Human Brain Mapping, 16*(4), 228-250. [PubMed]

Curcio, C. A., Sloan, K. R., Jr., Packer, O., Hendrickson, A. E., & Kalina, R. E. (1987). Distribution of cones in human and monkey retina: individual variability and radial asymmetry. *Science, 236*(4801), 579-582. [PubMed]

Curcio, C. A., Sloan, K. R., Kalina, R. E., & Hendrickson, A. E. (1990). Human photoreceptor topography. *Journal of Comparative Neurology, 292*(4), 497-523. [PubMed]

DeYoe, E. A., Carman, G. J., Bandettini, P., Glickman, S., Wieser, J., Cox, R., Miller, D., & Neitz, J. (1996). Mapping striate and extrastriate visual areas in human cerebral cortex. *Proceedings of the National Academy of Sciences (USA), 93*, 2382-2386. [PubMed] [Article]

Dumoulin, S. O., Baker, C. L., Jr., & Hess, R. F. (2001). Centrifugal bias for second-order but not first-order motion. *Journal of the Optical Society of America A 18*(9), 2179-2189. [PubMed]

Duncan, R. O., & Boynton, G. M. (2002). Cortical magnification factor in human primary visual cortex correlates with Vernier acuity thresholds [Abstract]. *Journal of Vision, 2*(7), 129a. http://journalofvision.org/2/7/129/, [Abstract]

Endo, S., Toyama, H., Kimura, Y., Ishii, K., Senda, M., Kiyosawa, M., & Uchiyama, A. (1997). Mapping visual field with positron emission tomography by mathematical modeling of the retinotopic organization in the calcarine cortex. *IEEE Transactions on Medical Imaging, 16*(3), 252-260. [PubMed]

Engel, S. A., Glover, G. H., & Wandell, B. A. (1997). Retinotopic organization in human visual cortex and the spatial precision of functional MRI. *Cerebral Cortex, 7*(2), 181-192. [PubMed]

Engel, S. A., Rumelhart, D. E., Wandell, B. A., Lee, A. T., Glover, G. H., Chichilnisky, E. J., & Shadlen, M. N. (1994). fMRI of human visual cortex [letter] [published erratum appears in Nature 1994 Jul 14;370(6485):106]. *Nature, 369*(6481), 525. [PubMed]

Filimonoff, I. N. (1932). Über die Variabilität der Grosshirnrindenstruktur. Regio occipitalis beim erwachsenen Menschen. *J. Psychol. Neurol., 44*, 1-96.

Fischer, B., & Modersitzki, J. (1999). Fast inversion of matrices arising in image processing. *Numerical Algorithms, 22*(1), 1-11.

Fischl, B., & Dale, A. M. (2000). Measuring the thickness of the human cerebral cortex from magnetic resonance images. *Proceedings of the National Academy of Sciences (USA), 97*(20), 11050-11055. [PubMed]

Gennari, F. (1782) in Francisci Gennari Parmensis Medicinae Doctoris Collegiati de Peculiari Structura Cerebri Nonnullisque Eius Morbis-Paucae Aliae Anatom. Observat. Accedunt. Parma, Italy: Regio Typographeo.

Glover, G. H. (1999). Simple analytic spiral K-space algorithm. *Magnetic Resonance in Medicine, 42*(2), 412-415. [PubMed]

Glover, G. H., & Lai, S. (1998). Self-navigated spiral fMRI: interleaved versus single-shot. *Magnetic Resonance in Medicine, 39*(3), 361-368. [PubMed]

Horton, J. C., & Hoyt, W. F. (1991). The representation of the visual field in human striate cortex. A revision of the classic Holmes map. *Archives of Ophthalmology, 109*(6), 816-824. [PubMed]

Nestares, O., & Heeger, D. J. (2000). Robust multiresolution alignment of MRI brain volumes. *Magnetic Resonance in Medicine, 43*(5), 705-715. [PubMed]

Roland, P. E., & Zilles, K. (1994). Brain atlases--a new research tool. *Trends in Neuroscience, 17*(11), 458-467. [PubMed]

Roland, P. E., & Zilles, K. (1996). The developing European computerized human brain database for all imaging modalities. *Neuroimage, 4*(3 Pt 2), S39-47. [PubMed]

Roland, P. E., & Zilles, K. (1998). Structural divisions and functional fields in the human cerebral cortex. *Brain research. Brain research reviews, 26*(2-3), 87-105. [PubMed]

Sereno, M. I., Dale, A. M., Reppas, J. B., Kwong, K. K., Belliveau, J. W., Brady, T. J., Rosen, B. R., & Tootell, R. B. (1995). Borders of multiple human visual areas in humans revealed by functional mri. *Science, 268*, 889-893. [PubMed]

Sereno, M. I., McDonald, C. T., & Allman, J. M. (1994). Analysis of retinotopic maps in extrastriate cortex. *Cerebral Cortex, 4*(6), 601-620. [PubMed]

Sincich, L. C., & Horton, J. C. (2002). Pale cytochrome oxidase stripes in V2 receive the richest projection from macaque striate cortex. *Journal of Comparative Neurology, 447*(1), 18-33. [PubMed]

Slotnick, S. D., Klein, S. A., Carney, T., & Sutter, E. E. (2001). Electrophysiological estimate of human cortical magnification. *Clinical Neurophysiology, 112*(7), 1349-1356. [PubMed]

Stensaas, S. S., Eddington, D. K., & Dobelle, W. H. (1974). The topography and variability of the primary visual cortex in man. *Journal of Neurosurgery, 40*(6), 747-755. [PubMed]

Talairach, J., & Tournoux, P. (1988). *Co-Planar Stereotaxic Atlas of the Human Brain*. New York: Thieme Medical Publishers.

Teo, P. C., Sapiro, G., & Wandell, B. A. (1997). Creating connected representations of cortical gray matter for functional MRI visualization. *IEEE Transactions on Medical Imaging, 16*(6), 852-863. [PubMed]

Tootell, R. B., Mendola, J. D., Hadjikhani, N. K., Ledden, P. J., Liu, A. K., Reppas, J. B., Sereno, M. I., & Dale, A. M. (1997). Functional analysis of V3A and related areas in human visual cortex. *Journal of Neuroscience, 17*(18), 7060-7078. [PubMed]

Van Essen, D. C., Lewis, J. W., Drury, H. A., Hadjikhani, N., Tootell, R. B., Bakircioglu, M., & Miller, M. I. (2001). Mapping visual cortex in monkeys and humans using surface-based atlases. *Vision Research, 41*(10-11), 1359-1378. [PubMed]

Van Essen, D. C., Newsome, W. T., Maunsell, J. H., & Bixby, J. L. (1986). The projections from striate cortex (V1) to areas V2 and V3 in the macaque monkey: asymmetries, areal boundaries, and patchy connections. *Journal of Comparative Neurology, 244*(4), 451-480. [PubMed]

Wandell, B. A., Chial, S., & Backus, B. (2000). Visualization and Measurement of the Cortical Surface. *Journal of Cognitive Neuroscience, 12*(5), 739-752. [PubMed]